Am J Transl Res 2019;11(4):2028-2041
www.ajtr.org /ISSN:1943-8141/AJTR0084123

Original Article

Evaluation of intervertebral disc regeneration with injection of mesenchymal stem cells encapsulated in PEGDA-microcryogel delivery system using quantitative T2 mapping: a study in canines

Jinwei Ying[1,2,3*], Zhihua Han[4,5*], Yang Zeng[6*], Yanan Du[7], Shishen Pei[1,2], Linghao Su[1,2], Dike Ruan[1,2], Chun Chen[3,8]

[1]The Second School of Clinical Medicine, Southern Medical University, Guangzhou 510515, China; [2]Department of Orthopedic Surgery, Navy General Hospital, Beijing 100048, China; [3]Department of Orthopedic Surgery, The First Affiliated Hospital of Wenzhou Medical University, Wenzhou 325000, China; [4]Department of Trauma and Orthopedics, Trauma Center, Shanghai General Hospital, School of Medicine, Shanghai Jiao Tong University, Shanghai, China; [5]Experimental Trauma and Orthopedic Surgery, JW Goethe-University, Frankfurt am Main, Germany; [6]Department of Cancer Biology, Dana Farber Cancer Institute/Harvard Medical School, 360 Longwood Ave, Room 3316K, Boston, MA; [7]Department of Biomedical Engineering, Collaborative Innovation Center for Diagnosis and Treatment of Infectious Diseases, School of Medicine, Tsinghua University, Beijing 100084, China; [8]Engineering Research Center of Clinical Functional Materials and Diagnosis and Treatment Devices of Zhejiang Province, Wenzhou Institute of Biomaterials and Engineering, Wenzhou 325011, China. [*]Equal contributors.

Received August 16, 2018; Accepted January 29, 2019; Epub April 15, 2019; Published April 30, 2019

Abstract: Intervertebral disc degeneration (IDD), the primary cause of low back pain, is still a great challenge to spinal surgeons and clinicians. T2 mapping, a biochemical magnetic resonance imaging (MRI) technique to calculate relaxation time, has the potential to offer a quantitative assessment of IDD. The aim of the study was to evaluate the regenerative effects of adipose-derived mesenchymal stem cells (MSCs) encapsulated in PEGDA-microcryogels (PMs) reinforced alginate hydrogel (AH) on the degenerative intervertebral disc (IVD) in a canine model using T2 mapping. Four degeneration-induced IVDs (L3-L4 to L6-L7) of 12 adult beagle dogs were injected with phosphate-buffered saline (PBS), MSCs, AH-PMs, and MSCs-laden AH-PMs, respectively. The intact IVD L7-S1 served as the normal control. IVD height change on plain radiograph, Pfirrmann grade and T2 relaxation time on MRI, histological change, and extracellular matrix (ECM)-associated proteins were evaluated during the 24-week follow-up period. Injection of MSCs-laden AH-PMs had the most satisfactory effects, having less decrease of IVD height, lower Pfirrmann grade, milder histological change, and longer T2 relaxation time ($P < 0.05$). T2 relaxation time was positively correlated with ECM content (proteoglycan: $r = 0.85$, $P < 0.001$; collagen II: $r = 0.79$, $P < 0.001$) and IVD height ($r = 0.81$, $P < 0.001$), but negatively correlated with Pfirrmann grade and histological grade (rho = -0.86, $P < 0.001$; rho = -0.95, $P < 0.001$). These results suggest that T2 mapping has the potential to quantitatively evaluate the repairing effects of cell-based engineering treatments on IDD for a long-term follow-up.

Keywords: T2 mapping, intervertebral disc regeneration, mesenchymal stromal cell, microcryogels, tissue engineering

Introduction

Intervertebral disc degeneration (IDD) is the most common cause of low back pain (LBP), which may cause disabilities in adults along with an enormous socioeconomic burden [1]. Although the exact pathogenesis of IDD remains unclear, it is primarily caused by the decrease of water and extracellular matrix (ECM) content in the nucleus pulposus (NP) as well as the loss of the collagen structure, eventually leading to alterations in morphological and biomechanical properties [2].

Despite the high incidence of IDD, current treatments, such as conservative and surgical treat-

ments, are confined to alleviate the symptoms rather than to address the underlying causes of degeneration and repair the intervertebral disc (IVD) structure or function [3]. Transplantation of bone marrow-derived mesenchymal stem cells (MSCs) holds a great promise for IVD regeneration because of their self-renewal ability and multilineage differentiation potential, focusing on regulating matrix production and restoring the IVD function [4-6]. Alternatively, adipose-derived MSCs have been proved to be another potential cell source for promoting IVD regeneration due to a more easily accessible and abundant source [7, 8]. However, the transplanted MSCs might not fully implement their therapeutic function because the hostile microenvironment of the degenerative IVD impairs their survival and function [9, 10]. In addition, cell leakage due to the high internal pressure in the degenerative IVD may cause osteophyte formation leading to deteriorate the degenerative state [11]. It has been broadly proved that biomaterial scaffolds could provide suitable conditions for MSCs to differentiate into metabolically active NP-like cells facilitating IVD regeneration [12-15]. In our previous study, we developed an injectable microscale 3D cell scaffold as the carrier for MSCs, composed of alginate hydrogel (AH) and Poly (ethylene glycol) diacrylate (PEGDA)-microcryogels (PMs), which could induce the encapsulated MSCs to express chondrocyte-like phenotypes *in vitro* [13].

Although cell-based tissue engineering treatments have become promising to clinical application, there still lack of reliable and precise tools to monitor the therapeutic effects. As is well-known, it is inevitable to evaluate the histological and biochemical changes in the degenerative IVD using laboratory tests in addition to radiological evaluations in clinical settings. However, these invasive laboratory tests demand of sacrificing the animals and harvesting the samples. Therefore, developing a reliable and non-invasive tool to quantify the changes of intrinsic properties of the IVD is of critical importance to advance the cell-based treatment of IDD.

T2 mapping has emerged to be able to adequately identify the biochemical composition and histological changes of the cartilaginous tissue, for it is highly sensitive to hydration and collagen structure [16-18]. It has been reported that T2 mapping could quantitatively assess early changes in the composition of various cartilaginous tissues, such as articular cartilage and IVDs [19-21]. In addition, a strong negative correlation between T2 relaxation time and IVD degeneration had been reported previously [22-24]. Furthermore, T2 relaxation time showed a strong and significant correlation with the amount of proteoglycan (PG) within the IVDs [25]. These findings lay the foundation of applying T2 mapping to evaluate not only the change of biochemical components within the degenerative IVD but also the regenerative effects after treatment.

Therefore, the purpose of this study was to investigate the feasibility of T2 mapping for quantitatively assessing the repairing effects of injection of adipose-derived MSCs encapsulated in PEGDA-microcryogel delivery system into the degenerative IVD in a canine model.

Materials and methods

Fabrication of PMs

PMs were fabricated and collected following the protocol of previous studies [13, 26]. Firstly, a poly (methymethacrylate) (PMMA) microstencil array chip was designed and created as a micromold for PEGDA-microcryogel array chips. Then the microstencil array chips were filled with PEGDA precursor solution and underwent crygelation, lyophilization and washing. Subsequently, about 600 cylinder-shaped PMs were harvested from a microstencil array chip using an ejector pin array and collected by filtering through 70 μm cell strainer (BD Biosciences, USA). After collecting from the microstencil array chips, the PMs were dispersed into a 35 mm dish and formed a thin layer evenly for second time freeze about 4 to 24 h. Before autoloading cells, PMs (diameter = 400 μm; height = 300 μm) were freeze-dried and sterilized by ethylene oxide.

Auto-loading of MSCs into the microcryogels

Canine adipose tissue was collected from the inguinal region of 12 healthy adult beagle dogs (18-month, approximately 12 kg) under the approval of the Institutional Ethics Committee of Navy General Hospital, Beijing, China.

Isolation and culture of adipose-derived MSCs was based on the experimental procedure described in our previous study [13]. Cells in Passage 3 to 5 were used for following experiments. After digestion and centrifugation, 1 × 10^7 cells resuspended in 500 μl medium were mixed with 500 μl 2% w/v alginate sodium to constitute a final concentration of 1 × 10^7 cells/ml within 1% alginate hydrogel solution. Then 60 μl cell-alginate mixture was pipetted onto the surface of the microcryogels until thorough auto-absorption. Next, the cell-loaded microcryogels were immediately immersed into 100 mM $CaCl_2$ for gelation of the alginate precursor [27] and then washed twice with phosphate-buffered saline (PBS) before supplementing with culture medium. Separation of alginate hydrogel-loaded PMs (AH-PMs) into single microcellular niche was performed by gentle mechanical stirring on the following day of culture [13]. Medium was changed to remove dead cells after separation. Cell-laden AH-PMs were cultured for two days in MSC basal medium before injection into the NP tissue.

Cell viability

Live and dead staining was used to assess cell viability cultured in AH-PMs. MSCs with a cell density of 1 × 10^7 cells/ml in 1% alginate hydrogel solution were loaded into PMs. After seven days culture, the cells laden in AH-PMs were incubated with 2 mM fluorogenic ester calcein-AM (CAM, Dojindo, Japan) and 4.5 mM propidium iodide (PI, Sigma, Japan) for 30 min at room temperature in the dark and then were gently rinsed with PBS three times. A confocal microscope (LSM710, Zeiss, Germany) was used to acquire images, and the numbers of live and dead cells were counted in five random fields. The experiments were repeated three times and the results were averaged for analysis.

Labelling MSCs with lentiviruses expressing GFP or co-expressing GFP and luciferase (Luc)

To assess the cell distribution in the IVD motion segments *ex vivo* and the cell viability in the degenerative IVDs *in vivo* after injection, the cultured MSCs were transfected with lentiviruses expressing GFP or Luc-GFP. The detailed transduction protocol was based on the method described by Rick *et al.* [28]. Briefly, MSCs seeded in 6-well plates were transfected with lentiviral vectors encoding eGFP or Luc-eGFP (purchased from Genechem Co., Ltd., Shanghai). After 24 h, the transfection medium was removed and replaced with MSC basal medium. After five days of culture, the transfected cells were collected to evaluate the positive rate of GFP or Luc-GFP. The MSCs transfected with GFP or Luc-GFP were used for the following experiments.

Leak-proof capacity test

To evaluate the leak-proof capacity of PMs, the IVD organs were harvested from the beagle dogs in another research project as the healthy control for *ex vivo* injection experiment. After removal of soft tissue and posterior structure, about 20 mg NP tissue of each IVD organ was aspirated by 10 ml syringe with 21-gauge needle to leave a space for cells or cell-microcryogels injection. Briefly, 40 μl cell suspension of 1 × 10^5 GFP^+ MSCs or Luc-GFP^+ with or without AH-PMs was injected into the NP tissue of all IVD motion units. To track injected cells upon delivery, bioluminescent live imaging was performed by Lumina IVIS (Caliper Life Sciences, Mountain View, CA) to evaluate cell distribution immediately after injection.

Animal experiments

All animal experiments were carried out under the approval of the Institutional Ethics Committee of Navy General Hospital, Beijing, China. A reproducible, progressive IDD model was performed under general anesthesia (Ketamine 10 mg/kg and Midazolam 0.5 mg/kg) [29]. The NP tissue from the lumbar IVDs (L3-L4 to L6-L7) of the 12 beagle dogs was aspirated through a left-side anterolateral approach using a 21-gauge needle with a 10 ml syringe, as described by Hiyama *et al.* [30]. The aspirated IVD fragments were carefully examined to confirm only the NP was aspirated. The average weight of the aspirated NP tissue from each IVD was about 21 ± 2.4 mg. These four aspirated IVDs were included into the degenerative groups. All animals had no neurological defect and stayed alive during the observation period (24 weeks).

Four weeks later, the four degeneration-induced IVDs were treated differently through a right-side anterolateral approach: L3-L4 was injected with PBS (sham group); L4-L5 was injected with 40 μl of 1 × 10^5 GFP^+ MSCs (MSCs group); L5-L6 was injected with 40 μl AH rein-

forced by PMs without cells (AH-PMs group); L6-L7 was injected with 40 μl of 1 × 10^5 GFP^+ MSCs incorporated in AH-PMs (MSCs + AH-PMs group). L4-L5, L5-L6, and L6-L7 were regarded as the treatment groups. The intact IVD L7-S1 without operation served as the normal control (NC group). All animals were evaluated at 4, 8, 12, and 24 weeks after treatment.

Radiography

Standard lateral plain radiographs for the lumbar spine were taken under general anesthesia (Ketamine 10 mg/kg and Midazolam 0.5 mg/kg). Disc height index (DHI) was calculated according to the measurement established by Lu *et al.* [31]. In short, the average IVD height was calculated by averaging the measurements obtained from anterior, middle and posterior portions of the IVD. DHI was calculated from average IVD height divided by the average of adjacent vertebral body heights. The Change of IVD height was expressed as % DHI normalized to the measured preoperative IVD heights (Figure S1). All radiographic images were independently interpreted and measured by two blinded radiologists who didn't participate in the animal experiment. In case of discrepancy, they would turn to an orthopedic surgeon with 30-year experience for a final decision.

MRI

A 3.0-T MR scanner (GE Signa Echo-Speed; GE Medical Systems, Milwaukee WI) was used for all MRI examinations. The beagle dogs were placed supine on a quadrature surface. T2-weighted images on the sagittal plane were used for morphological evaluation of IVD degeneration according to Pfirrmann grading system [32] at 12 and 24 weeks after operation. T2 relaxation time were achieved by manually drawing the regions of interest (ROIs) to outline the area of the NP tissue on the mid-sagittal T2-weighted images. Then the ROIs were copied and pasted onto the corresponding T2 mapping images [33, 34]. The mean value of three repeated measurements was used for statistical analysis. Detailed parameters of MRI sequences are presented in Table S1. The T2 mapping scans were processed by an image work-station (ADW 4.3, Functool, GE Medical Systems, Milwaukee WI).

Histology

After the radiological evaluations, the dogs were euthanized by overdose of pentobarbital sodium (200 mg/kg). The IVDs (L3-L4 to L7-S1) were dissected from the spine and the attached soft tissue was carefully removed. Then each motion unit was cut into two equal parts along the mid-sagittal plane, one half was used for histological analysis while another half was used for biochemical analysis. For histological evaluation, the samples were fixed in 10% formalin for one week, followed by decalcification in 14% EDTA for 6 weeks. After decalcification, the samples were dehydrated in a graded series of ethanol and embedded in paraffin block. The block was cut into 4 μm slices. Para-middle slices were selected for hematoxylin and eosin (H&E), Safranin-O staining, and immunofluorescence. Histological score was evaluated by two independent researchers according to the validated histological grading scale (Table S2) [5, 35], which was characterized by the morphological changes in the structure of inner annulus fibrosus. Because reconstitution of annular structure is an important indicator for the therapeutic effect after treatment [5]. Any disagreement about the histological score would be solved through discussion to reach a consensus.

Immunofluorescence

Immunofluorescence was applied to evidence the retention of GFP-labelled cells within the IVDs at 24 weeks post treatment. The sections were incubated fluorescein isothiocyanate (FITC) conjugated anti-GFP (1:200, Abcam, USA) for 60 min at room temperature away from light. Then the sections were counterstained with DAPI (Beyotime Biotechnology, China) and mounted. The presence of the transplanted cells in the IVDs was observed under confocal microscopy (LSM710, Zeiss).

Enzyme-linked immunosorbent assay (ELISA)

Tissue samples were lysed by T-PER™ tissue protein extraction reagent (ThermoFisher Scientific, USA), and total protein concentration was quantified using BCA protein assay (Beyotime Biotechnology). The amounts of PG and collagen II (COL II) were quantified using

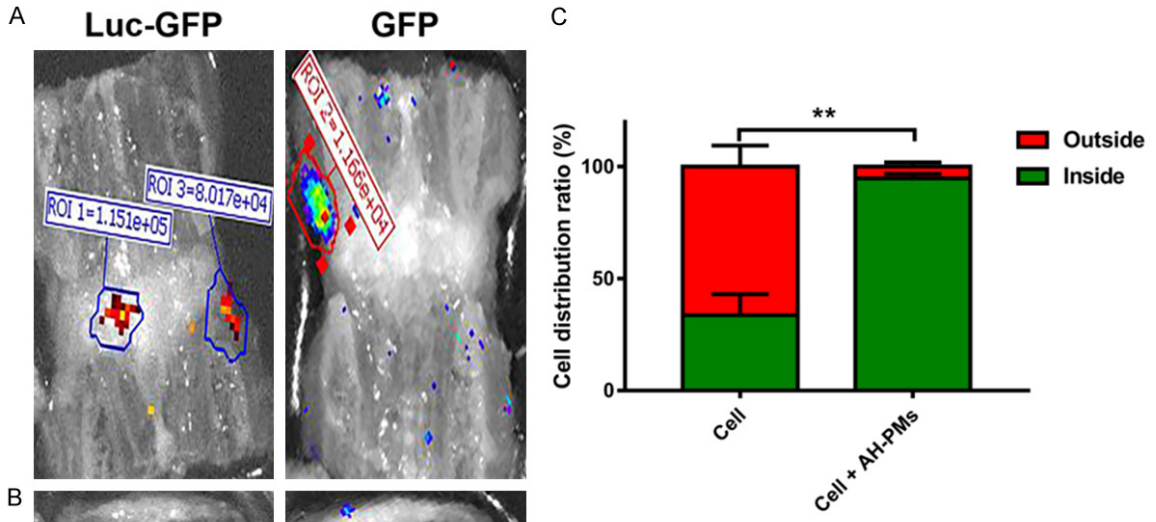

Figure 1. Bioluminescent images showing the leak-proof capacity of AH-PMs. A. Apparent leakage could be observed after injecting MSCs into the IVDs alone. B. No obvious cell leakage after delivery of MSCs assisted by AH-PMs. C. Quantitative comparison of cell distribution between cell injection alone and cell delivery assisted by AH-PMs. The mean ratios between inside and outside were 94.8% *vs.* 5.2% in MSCs + AH-PMs group and 33.6% *vs.* 66.4% in MSCs group. MSCs, mesenchymal stem cells; GFP, green fluorescent protein; Luc, luciferase; AH, alginate hydrogel; PMs, PEGDA-microcryogels; IVD, intervertebral disc. All data represent mean ± SD, n = 3. ** indicates P < 0.001.

ELISA kits (anti-canine antibodies, Shengxikang, China). All samples were assayed in triplicate.

Statistical analysis

Statistical analysis was performed using SPSS19.0 (SPSS, Chicago, Illinois, USA). All values are expressed as mean ± standard deviation (SD). One-way analysis of variance (*ANOVA*) and *post hoc test* (*Student-Newman-Keul* for homogeneity of variance or *Tamhane's test* for heterogeneity of variance) were used to compare T2 relaxation time among the five groups. The χ^2 test was used to compare the rates of live and dead cells cultured *in vitro,* the cell distribution in the IVD *ex vivo*, and the distribution of degenerative grades in different groups *in vivo*. *Pearson's correlation* was performed to reveal the correlation between T2 relaxation time and ECM content in the IVD. *Spearman's rank correlation* was applied to explore the correlation between T2 relaxation time and degenerative grades based on Pfirrmann and histological grades. $P < 0.05$ was considered as statistical significance.

Results

Characteristics of AH-PMs

The interconnected macroporous structure and microscale size enabled PMs to load alginate automatically and homogeneously via physical absorption in favor of cell-encapsulation. Particularly, this biomaterial scaffold was available for cellular remodelling and adherence (Figure S2). As shown in confocal images, MSCs were evenly distributed inside of AH-PMs after auto-loading and there were scarcely dead cells after 7-day culture *in vitro*, which might illustrate the low cytotoxicity of this biomaterial scaffold (Figure S3). To evaluate the capacities of leakage-proof and cell retention in AH-PMs, MSCs were successfully transfected with lentiviruses to express GFP or Luc-GFP (Figure S4). As proved by bioluminescent imaging, most of the cells leaked out of the IVDs after cell injec-

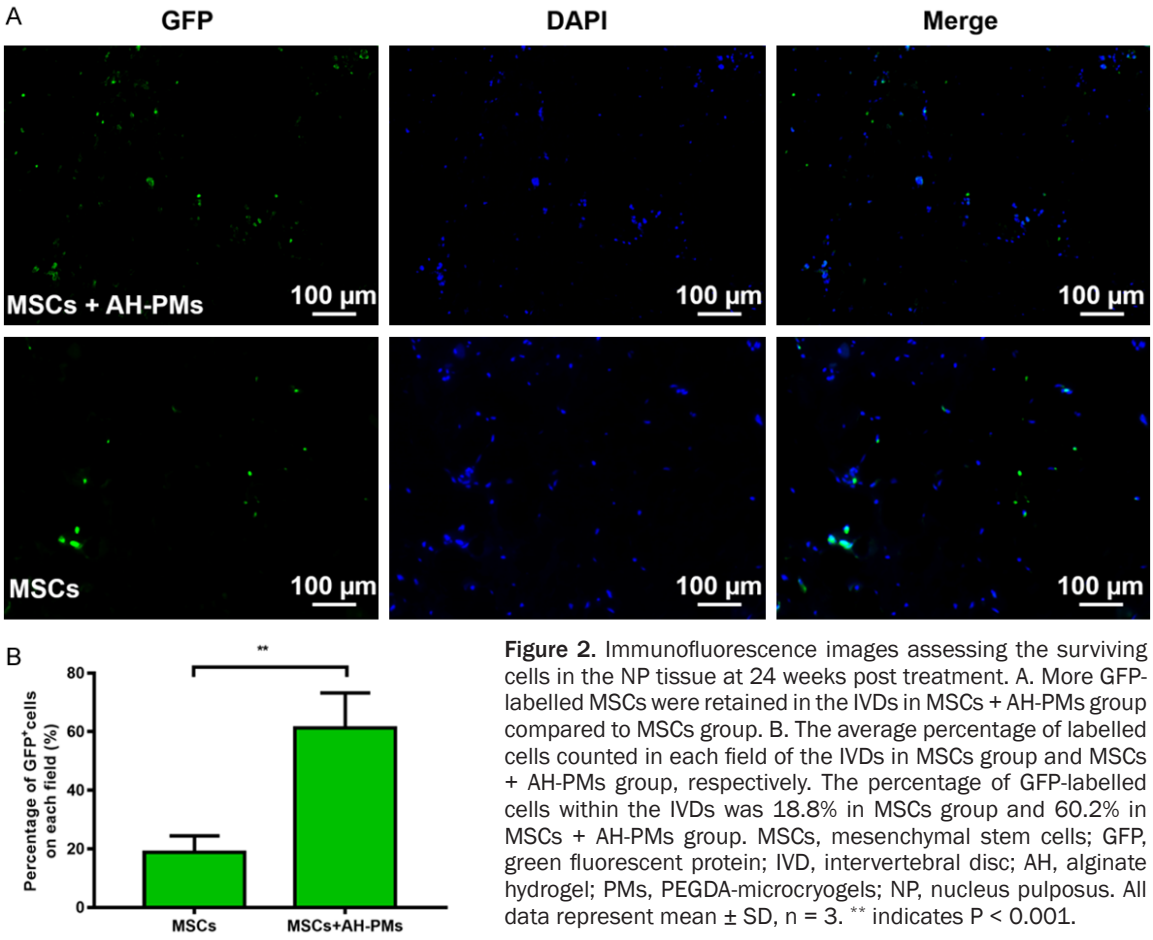

Figure 2. Immunofluorescence images assessing the surviving cells in the NP tissue at 24 weeks post treatment. A. More GFP-labelled MSCs were retained in the IVDs in MSCs + AH-PMs group compared to MSCs group. B. The average percentage of labelled cells counted in each field of the IVDs in MSCs group and MSCs + AH-PMs group, respectively. The percentage of GFP-labelled cells within the IVDs was 18.8% in MSCs group and 60.2% in MSCs + AH-PMs group. MSCs, mesenchymal stem cells; GFP, green fluorescent protein; IVD, intervertebral disc; AH, alginate hydrogel; PMs, PEGDA-microcryogels; NP, nucleus pulposus. All data represent mean ± SD, n = 3. ** indicates P < 0.001.

tion alone (**Figure 1A**). However, AH-PMs could assist cells delivery into the NP tissue availably without obvious leakage (**Figure 1B**). In the animal experiment, during the long-term follow-up, more GFP signal could be found in MSCs + AH-PMs group as long as 24 weeks, which demonstrated that more cells could retain and survive within the degenerative IVDs with the assistance of AH-PMs (**Figure 2**).

Change of IVD height

Although the IVD height decreased gradually in all groups after degeneration, MSCs-laden AH-PMs obviously slowed down the decreased rate of IVD height (P < 0.001). As shown in **Figure 3A**, the IVD height of the treatment groups decreased less than that of sham group without any intervention from 8 weeks post-operation (P < 0.001), and MSCs + AH-PMs group had less loss of IVD height compared to other treatment groups with MSCs or AH-PMs alone (P < 0.001). However, there was no difference in the IVD height between MSCs group and AH-PMs group from 8 weeks to 24 weeks after treatment (P > 0.05).

T2 relaxation time

T2 relaxation time in the IVDs treated with MSCs-laden AH-PMs decreased more slowly than other degenerative groups (**Figure 3B**). From 4 weeks post-operation, MSCs + AH-PMs group began to maintain higher T2 relaxation time than sham group (145.6 ± 9.2 ms *vs.* 129.7 ± 12.2 ms, P < 0.001), and the IVDs treated with only MSCs also had higher values than those without treatment (140.4 ± 6.3 ms *vs.* 129.7 ± 12.2 ms, P = 0.042). From 8 weeks post-operation, the significant difference could be found between MSCs + AH-PMs group and AH-PMs group (121.0 ± 8.3 ms *vs.* 107.7 ± 6.4 ms, P = 0.001). Meanwhile, the difference between AH-PMs group and sham group began to reach a statistical significance (107.7 ± 6.4 ms *vs.* 95.7 ± 7.1 ms, P = 0.002). During the whole follow-up, MSCs + AH-PMs group had the highest values among the treatment groups (P

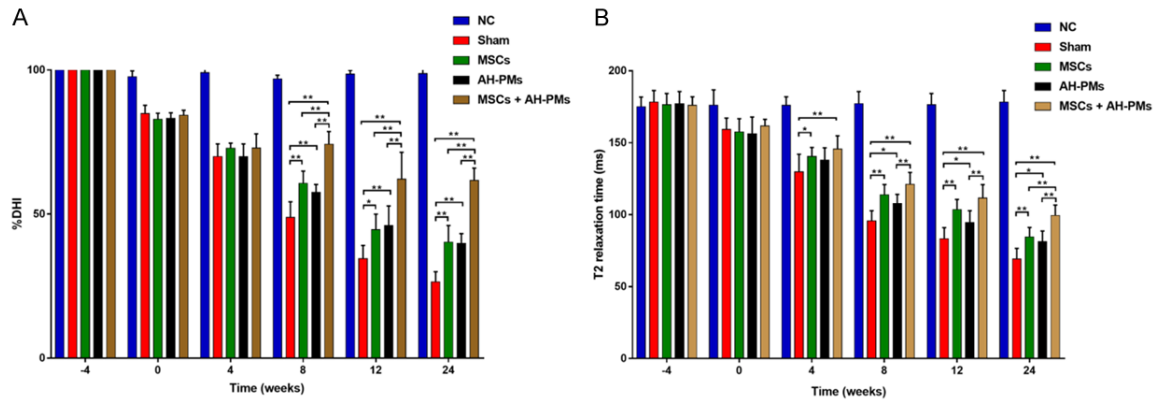

Figure 3. The changes of IVD height and T2 relaxation time after different treatments. A. The IVD height decreased gradually after degeneration. MSCs + AH-PMs group had higher IVD height compared to other treatment groups ($P < 0.001$). There was no difference in the IVD height between MSCs group and AH-PMs group ($P > 0.05$). B. T2 relaxation time decreased gradually after degeneration. MSCs + AH-PMs group had the highest T2 relaxation time after treatment ($P < 0.001$). After 8 weeks post-operation, the difference between AH-PMs group and sham group reached a statistical significance ($P = 0.002$). However, there was no significant difference between AH-PMs group and MSCs group ($P > 0.05$). IVD, intervertebral disc; NC, normal control; MSCs, mesenchymal stem cells; AH, alginate hydrogel; PMs, PEGDA-microcryogels; DHI, disc height index. All data represent mean ± SD, n = 12. * indicates $P < 0.05$, ** indicates $P < 0.001$.

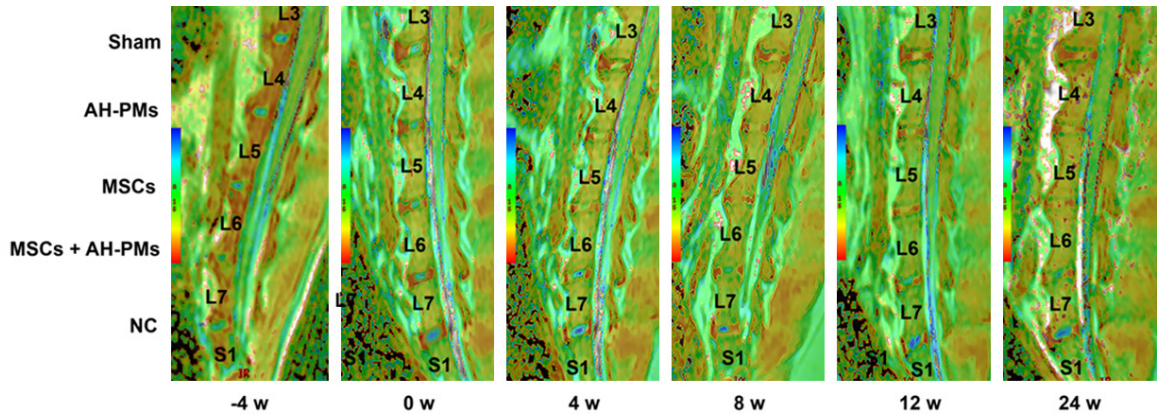

Figure 4. Representative serial T2 mapping images during the whole follow-up after treatment. Color-coded bar is shown in the left side. Blue indicates high T2 relaxation time while red indicates low T2 relaxation time. With development of degeneration and decrease of T2 relaxation time, the color shifted from blue to yellow or even red.

< 0.001) and no significant difference could be found between AH-PMs group and MSCs group ($P > 0.05$).

Moreover, the severity of IVD degeneration can be easily identified using T2 mapping because of the uniform color coding (**Figure 4**). The normal IVDs had a green to blue NP. With the development of degeneration, the color shifted toward yellow or even red accounting for the decreased T2 relaxation time. The IVDs treated with MSCs laden AH-PMs showed an analogous color to the normal IVDs but with slight changes. On the contrary, the color of degenerative IVDs without treatment turned to red. There was no obvious discrepancy between MSCs group and AH-PMs group as seen by the color ranging from green to yellow.

Similar to the decrease of IVD height, T2 relaxation time decreased gradually with the development of IVD degeneration (**Figure 3**). Statistically significant difference in T2 relaxation time could be firstly detected at 4 weeks after treatment. However, the first time for significant difference in IVD height appeared at 8 weeks after treatment. There was a significant correlation between T2 relaxation time and IVD height

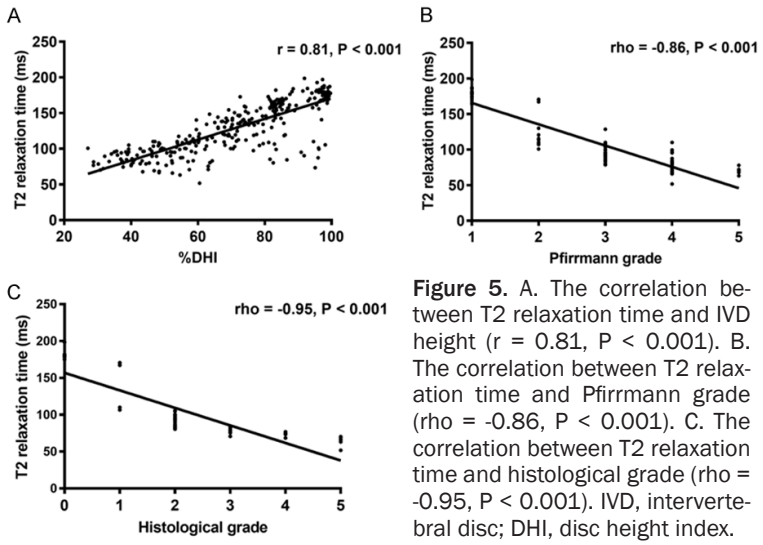

Figure 5. A. The correlation between T2 relaxation time and IVD height (r = 0.81, P < 0.001). B. The correlation between T2 relaxation time and Pfirrmann grade (rho = -0.86, P < 0.001). C. The correlation between T2 relaxation time and histological grade (rho = -0.95, P < 0.001). IVD, intervertebral disc; DHI, disc height index.

during the whole follow-up (r = 0.81, P < 0.001) (**Figure 5A**).

Pfirrmann grade

According to the Pfirrmann grading system, the severity of IVD degeneration in the four degenerative groups was different significantly at 12 and 24 weeks after treatment, respectively (χ^2 = 83.28, P < 0.001; χ^2 = 75.80, P < 0.001) (**Figure 6A**). The degenerative grade was lowest in MSCs + AH-PMs group among the treatment groups (P < 0.001). At 12 weeks after treatment, MSCs + AH-PMs group showed five IVDs graded II, seven IVDs graded III. Twelve weeks later, two of these IVDs developed to grade IV and others remained grade II or III. On the contrary, the degenerative IVDs in sham group without treatment showed the most severe degeneration (grade III = 6, grade IV = 4, grade V = 2 at 12 weeks; grade III = 1, grade IV = 8, grade V = 3 at 24 weeks). The moderate degeneration mainly appeared in the IVDs treated with MSCs or AH-PMs alone.

A total of 60 IVDs at the two time-points were included to analyze the correlation between T2 relaxation time and Pfirrmann grade. We demonstrated that T2 relaxation time was negatively correlated with Pfirrmann grade (rho = -0.86, P < 0.001) (**Figure 5B**). As shown in **Figure 6B**, T2 relaxation time decreased from 178.5 ± 7.6 ms at Pfirrmann grade I to 70.4 ± 4.9 ms at Pfirrmann grade V. Furthermore, the significant differences in T2 relaxation time could be observed among the lower Pfirrmann grades (grade I *vs.* grade II: 178.5 ± 7.6 ms *vs.* 128.6 ± 27.3 ms, P < 0.001; grade II *vs.* grade III: 128.6 ± 27.3 ms *vs.* 95.7 ± 10.5 ms, P < 0.001; grade III *vs.* grade IV: 95.7 ± 10.5 ms *vs.* 81.3 ± 12.0 ms, P < 0.001). However, the difference between higher Pfirrmann grades was not significant (grade IV: 81.3 ± 12.0 ms *vs.* grade V: 70.4 ± 4.9 ms, P = 0.568).

Histological assessment

According to histological grading system regarding the intactness of annulus fibrosus [5, 35], there was a significant difference in the distribution of histological changes among the different groups (χ^2 = 117.18, P < 0.001) (**Table 1**). As shown in **Figure 7**, the degenerative IVDs treated with MSCs-laden AH-PMs demonstrated the most satisfactory improvement with an approximate normal-looking or a slightly wavy inner annulus fibrosus, while the degenerative IVDs in sham group with no treatment showed severely serpentine or even indistinct appearance of annulus fibrosus. MSCs group and AH-PMs group showed moderately serpentine inner annulus fibrosus.

There was a stepwise decrease of T2 relaxation time with the increased histological grades (rho = -0.95, P < 0.001) (**Figure 5C**). However, the significant differences in T2 relaxation time only could be found between grade 0 and 1 (178.3 ± 7.9 ms *vs.* 108.3 ± 2.6 ms, P < 0.001), grade 1 and 2 (108.3 ± 2.6 ms *vs.* 91.8 ± 8.0 ms, P = 0.031), and grade 2 and 3 (91.8 ± 8.0 ms *vs.* 78.4 ± 4.2 ms, P < 0.001), but there were no significant differences between grade 3 and 4 (78.4 ± 4.2 ms *vs.* 72.2 ± 3.9 ms, P > 0.05), and between grade 4 and 5 (72.2 ± 3.9 ms *vs.* 64.5 ± 6.7 ms, P > 0.05) (**Figure 6C**).

The expression of ECM content

The degenerative IVDs treated with MSCs-laden AH-PMs showed higher levels of PG and COL II than other treatment groups (Table S3). Regarding the amount of PG, there were significant differences between MSCs + AH-PMs group and sham group (129.3 ± 27.5 pg/mg *vs.*

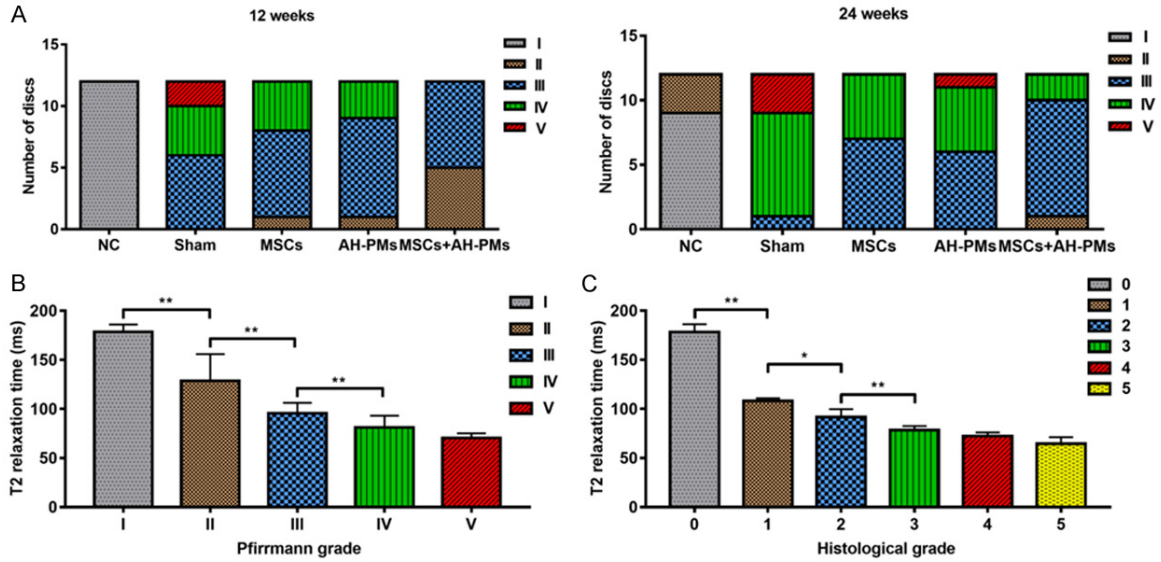

Figure 6. A. The distribution of degenerative grades of the IVDs according to Pfirrmann grading system at 12 weeks and 24 weeks after operation. There were significant differences in the numbers of different degenerative degrees at 12 and 24 weeks after treatment ($\chi^2 = 83.28$, $P < 0.001$; $\chi^2 = 75.80$, $P < 0.001$). B. Comparisons of T2 relaxation time in different Pfirrmann grades. The significant differences in T2 relaxation time could be found among Pfirrmann grade I-IV ($P < 0.001$) but could not be found between Pfirrmann grade IV and V ($P = 0.568$). C. Comparisons of T2 relaxation time in different histological grades. The significant differences in T2 relaxation time could be found between lower histological grades ($P < 0.05$). However, the differences in T2 relaxation time between higher histological grades were not significant ($P > 0.05$). IVD, intervertebral disc; NC, normal control; MSCs, mesenchymal stem cells; AH, alginate hydrogel; PMs, PEGDA-microcryogels. All data are expressed as mean ± SD, * $P < 0.05$, ** $P < 0.001$.

Table 1. T2 relaxation time and the number of different histological grades after treatment

Histology	NC	Sham	MSCs	AH-PMs	MSCs + AH-PMs	T2 relaxation time (ms)
0	12	0	0	0	0	178.3 ± 7.9
1	0	0	0	0	2	108.3 ± 2.6
2	0	0	6	8	9	91.8 ± 8.0
3	0	2	6	3	1	78.4 ± 4.2
4	0	4	0	1	0	72.2 ± 3.9
5	0	6	0	0	0	64.5 ± 6.7

NC, normal control; MSCs, mesenchymal stem cells; AH, alginate hydrogel; PMs, PEGDA-microcryogels.

72.2 ± 11.4 pg/mg, $P < 0.001$), between MSCs group and sham group (105.0 ± 13.1 pg/mg *vs.* 72.2 ± 11.4 pg/mg, $P = 0.023$), and between AH-PMs group and sham group (101.8 ± 13.9 pg/mg *vs.* 72.2 ± 11.4 pg/mg, $P = 0.045$). However, no statistical significance was found between MSCs group and AH-PMs group (105.0 ± 13.1 *vs.* 101.8 ± 13.9 pg/mg, $P = 0.103$). Compared to MSCs + AH-PMs group, both MSCs group and AH-PMs group had similar protein content of PG ($P = 0.212$; $P = 0.098$). Additionally, the expression of COL II had a similar trend to that of PG. Among the treatment groups, the expression level of COL II in MSCs + AH-PMs group was 113.9 ± 23.4 pg/mg, which was significantly higher than that in sham group (61.0 ± 10.6 pg/mg, $P < 0.001$), MSCs group (89.1 ± 10.5 pg/mg, $P = 0.003$), and AH-PMs group (82.0 ± 12.2 pg/mg, $P < 0.001$).

In addition, the IVDs treated with MSCs or AH-PMs alone also could retard the loss of COL II because the amount of COL II in MSCs or AH-PMs group was greater than that in sham group (89.2 ± 10.5 pg/mg *vs.* 61.0 ± 10.6 pg/mg, $P < 0.001$; 82.0 ± 12.2 pg/mg *vs.* 61.0 ± 10.6 pg/mg, $P = 0.016$). However, there was no significant difference between MSCs group and AH-PMs group (89.2 ± 10.5 pg/mg *vs.* 82.0 ± 12.2 pg/mg, $P > 0.05$). Compared to MSCs or AH-PMs alone, the composite of MSCs with AH-PMs had the advantage of promoting the expression of COL II significantly (113.9 ± 23.4 pg/mg *vs.* 89.2 ±

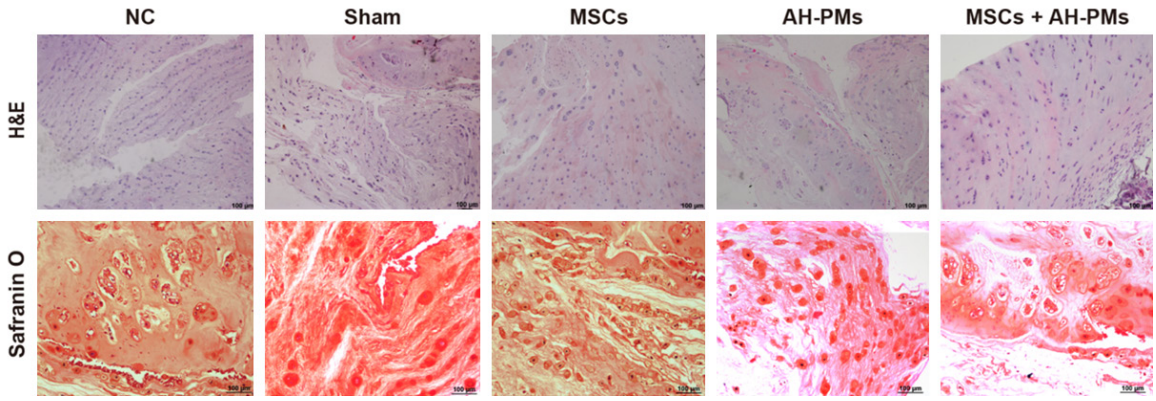

Figure 7. Histological evaluation of the structure changes in the IVDs using H&E and Safranin O after treatment. The degenerative IVDs treated with MSCs-laden AH-PMs had the most satisfactory recovery with a mild change in the annulus fibrosus, while the degenerative IVDs without treatment showed the most severe degeneration with ruptured or even indistinct annulus fibrosus and loss of proteoglycan. The degenerative IVDs treated with MSCs or AH-PMs alone had an improved condition but with various degrees of fibrotic or serpentine annulus fibrosus. IVD, intervertebral disc; H&E, hematoxylin and eosin; MSCs, mesenchymal stem cells; AH, alginate hydrogel; PMs, PEGDA-microcryogels.

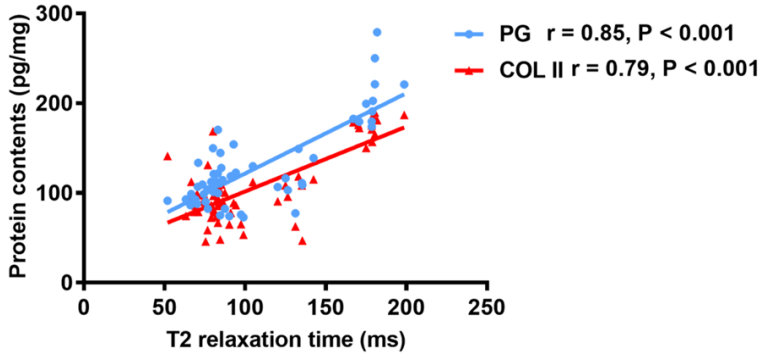

Figure 8. Correlations of T2 relaxation time with PG and COL II in the NP tissue after treatment. T2 relaxation time was significantly correlated with PG ($r = 0.85$, $P < 0.001$) and COL II ($r = 0.79$, $P < 0.001$). PG, proteoglycan; COL II, collagen II; NP, nucleus pulposus; NC, normal control; MSCs, mesenchymal stem cells; AH, alginate hydrogel; PMs, PEGDA-microcryogels. All data are expressed mean ± SD, n = 12, * indicates $P < 0.05$, ** indicates $P < 0.001$.

10.5 pg/mg, $P = 0.003$; 113.9 ± 23.4 pg/mg *vs.* 82.0 ± 12.2 pg/mg, $P < 0.001$).

As shown in **Figure 8**, T2 relaxation time was positively correlated with the amounts of PG and COL II. We found a stronger correlation between T2 relaxation time and the amount of PG than the correlation between T2 relaxation time and the expression of COL II (PG: $r = 0.85$, $P < 0.001$; COL II: $r = 0.79$, $P < 0.001$).

Discussion

The present study demonstrated PEGDA-microcryogel delivery system was able to amply encapsulate MSCs with low cytotoxicity and high leakage-proof that significantly improved cell retention and survival within the degenerative IVDs, which might provide 3D microscale niches and excellent mechanical support for the loaded cells [13]. In addition, MSCs-laden AH-PMs was effective for treatment of IDD in a canine model, as demonstrated by not only histological and biochemical analyses in the laboratory but also radiological measurements in clinical settings. However, these laboratory tests are invasive that demand of sacrificing the animals and collecting the samples, and signal intensity on conventional MRI was limited in detecting early signs of degeneration [16, 32]. Therefore, we evaluated the feasibility of T2 mapping as a non-invasive tool of detecting regeneration of the degenerative IVD after treatment.

We demonstrated the significant therapeutic effect of MSCs-laden AH-PMs on the treatment for IDD. Although MSCs or AH-PMs could reduce the loss of IVD height, MSCs incorporated into AH-PMs achieved significantly better effect than MSCs or AH-PMs alone. Furthermore, MSCs-laden AH-PMs showed the best capacity

of retarding the IVD degenerative progress in Pfirrmann grade, because the IVDs almost stayed at grade III, only two IVDs progressed to grade IV at the end of follow-up. The similar results were also found in histological evaluation, the IVDs treated by MSCs-laden AH-PMs showed a significant improvement in the annular structure. Moreover, MSCs + AH-PMs group showed a significant increase of PG and COL II content. On one hand, AH-PMs itself could provide mechanical support [13] and protect the loaded cells from the harsh environment within the degenerative IVD contributing to their growth and differentiation [36]. On the other hand, MSCs were able to differentiate towards NP-like and secret NP-related ECM [37]. Therefore, AH-PMs group gave an impression of improvement similar to MSCs group with obvious increase of PG and COL II expression compared to sham group.

Changes in the biochemical properties in the NP, characterized by the reduction of water and PG content, are some of the first known factors and important indicators for early IDD prior to the gross structural changes [38, 39]. T2 mapping as an emerging quantitative MRI technique could adequately reflect the biochemical composition and histological grading of the corresponding tissue, as it is highly sensitive to hydration and collagen structure [16-18]. Cai *et al.* [25] reported that T2 relaxation time in the NP increased with the increased ECM expression after MSCs transplantation. Peeters *et al.* [40] evaluated the safety and efficacy of BMPs conjugated to one hydrogel for IVD regeneration in a goat IDD model and demonstrated a strong and significant correlation between T2 relaxation time and biochemical content in ECM. Thus, T2 mapping may be a promising method to monitor the repairing effects of regenerative treatments on IDD in the early stage through evaluating the ECM reconstruction.

Consistent with the results of radiography, signal intensity, histological and biochemical analyses, we found that IVDs treated by MSCs-laden AH-PMs obtained the highest T2 relaxation time among the degenerative IVDs after treatment. There was no significant difference in T2 relaxation time between AH-PMs group and MSCs group, but both of them showed significant higher values than sham group. These findings indicate that AH-PMs could be an ideal candidate biomaterial scaffold for future clinical application.

The results of significant correlations between T2 relaxation time and other parameters suggest the applicability of T2 mapping as a reliable tool for monitoring the effects of cell-based engineering treatments. As previously reported, T2 relaxation time was negatively correlated to Pfirrmann grade [21, 25, 41]. It is noteworthy that T2 relaxation time is more sensitive to distinguish the early or middle stage of IDD rather than the end stage of degeneration, because the significant differences could be found among Pfirrmann grade I-IV, but could not be found between Pfirrmann grade IV and V. Watanabe *et al.* [16] also found an insignificant decrease of T2 relaxation time between higher Pfirrmann grades. The smaller number of higher degenerative grades in our study might lead to the insignificant difference in T2 relaxation time between grade IV and V. However, such sensitivity allows T2 mapping to effectively identify IVD degeneration in the early stage, which is the proper period for cell-based therapy, while the late stage usually requires surgical intervention [3, 42].

Likewise, we found a significant positive correlation between T2 relaxation time and IVD height. It's important to note that the significant differences in T2 relaxation time were found 4 weeks earlier than IVD height change after treatment, indicating that T2 mapping is more suitable to evaluate the regenerative effects in the early period after treatment. This discrepancy might be caused by minimal or even no change of IVD height occurring in the early stage of IDD, or varying muscle relaxation and positioning affecting the measurement of IVD height on plain radiograph [41].

Furthermore, the correlations of T2 relaxation time with PG and COL II content proved the applicability of T2 mapping to monitor the regenerative effects after cell-based tissue engineering treatments. The expression levels of PG and COL II would be affected by the homeostatic imbalance between anabolism and catabolism during IDD [2, 38, 39]. The decrease of PG and COL II content was considered as important indicator of IDD [43]. Since the significant correlations were found between

T2 relaxation time and the expression of PG and COL II, T2 mapping has the ability to reflect the changes of the ECM content. Additionally, we found that the correlation between T2 relaxation time and PG was stronger than that between T2 relaxation time and COL II. These similar findings were also reported in other previous studies [25, 44, 45]. A possible reason for this might be that PG is much greater than COL II within the NP tissue [46] and PG has more powerful water retaining capacity, thus the change of PG content can be more accurately reflected on T2 relaxation time. This also suggests that T2 relaxation time can reveal biochemical changes in the NP tissue after treatment.

However, there are several limitations in this research. Firstly, this animal model only provided an acute IDD model, which may not truly represent the nature chronic process of IDD in human. Secondly, other studies [33, 47] recommended dividing the IVD into some specific regions for ROIs placements and data measurements, but we only measured the T2 relaxation time in the NP tissue to reflect the biochemical changes of the whole IVD in the early stage. Because the earlier degenerative changes typically occur in the NP tissue [48] and the IDD animal model in our study was also created in the early stage. Thirdly, to avoid the incomparability caused by the numbers of lower and higher Pfirrmann grades, the data of T2 relaxation time in the early period after treatment was not included for statistical analysis. Furthermore, future research should compare T2 mapping with other quantitative imaging techniques such as T1ρ or diffusion tensor imaging [49, 50], to select the best option for clinical practice.

In conclusion, our study demonstrated that MSCs-based PEGDA-microcryogel delivery system might offer a promising clinical application to attenuate IVD degeneration in regenerative medicine. As consistent with biochemical and histological analyses, T2 relaxation time might have the potential to reflect the ECM content. Therefore, T2 mapping holds a great promise to be a non-invasive and quantitative tool for diagnosis of degenerative IVD diseases and evaluation of regenerative effects on IDD after treatment in the clinical setting.

Acknowledgements

This work was supported by the National Natural Science Foundation of China (81702132 and 81772399), the Projects of Medical and Health Technology Program in Zhejiang province (2017KY456), and the Wenzhou Public Welfare Science and Technology Research Project (Y20160130). The authors thank Department of Biomedical Engineering, Tsinghua University for providing the equipment of biomaterial preparation and testing.

Disclosure of conflict of interest

None.

Address correspondence to: Dike Ruan, Department of Orthopedic Surgery, Navy General Hospital, Fucheng Road, Haidian District, Beijing 100048, China. E-mail: ruandikengh@163.com; Chun Chen, Department of Orthopedic Surgery, The First Affiliated Hospital of Wenzhou Medical University, Nan Baixiang Road, Wenzhou 325000, China. E-mail: chenchunkk@163.com

References

[1] Natarajan RN, Andersson GB, Patwardhan AG and Andriacchi TP. Study on effect of graded facetectomy on change in lumbar motion segment torsional flexibility using three-dimensional continuum contact representation for facet joints. J Biomech Eng 1999; 121: 215-221.

[2] Buckwalter JA. Aging and degeneration of the human intervertebral disc. Spine (Phila Pa 1976) 1995; 20: 1307-1314.

[3] May M. Regenerative medicine: rebuilding the backbone. Nature 2013; 503: S7-9.

[4] Bendtsen M, Bunger CE, Zou X, Foldager C and Jorgensen HS. Autologous stem cell therapy maintains vertebral blood flow and contrast diffusion through the endplate in experimental intervertebral disc degeneration. Spine (Phila Pa 1976) 2011; 36: E373-379.

[5] Sakai D, Mochida J, Iwashina T, Hiyama A, Omi H, Imai M, Nakai T, Ando K and Hotta T. Regenerative effects of transplanting mesenchymal stem cells embedded in atelocollagen to the degenerated intervertebral disc. Biomaterials 2006; 27: 335-345.

[6] Sakai D, Mochida J, Yamamoto Y, Nomura T, Okuma M, Nishimura K, Nakai T, Ando K and Hotta T. Transplantation of mesenchymal stem cells embedded in atelocollagen gel to the intervertebral disc: a potential therapeutic mod-

el for disc degeneration. Biomaterials 2003; 24: 3531-3541.
[7] Ganey T, Hutton WC, Moseley T, Hedrick M and Meisel HJ. Intervertebral disc repair using adipose tissue-derived stem and regenerative cells: experiments in a canine model. Spine (Phila Pa 1976) 2009; 34: 2297-2304.
[8] Hoogendoorn RJ, Lu ZF, Kroeze RJ, Bank RA, Wuisman PI and Helder MN. Adipose stem cells for intervertebral disc regeneration: current status and concepts for the future. J Cell Mol Med 2008; 12: 2205-2216.
[9] Sakai D and Andersson GB. Stem cell therapy for intervertebral disc regeneration: obstacles and solutions. Nat Rev Rheumatol 2015; 11: 243-256.
[10] Huang YC, Leung VY, Lu WW and Luk KD. The effects of microenvironment in mesenchymal stem cell-based regeneration of intervertebral disc. Spine J 2013; 13: 352-362.
[11] Vadala G, Sowa G, Hubert M, Gilbertson LG, Denaro V and Kang JD. Mesenchymal stem cells injection in degenerated intervertebral disc: cell leakage may induce osteophyte formation. J Tissue Eng Regen Med 2012; 6: 348-355.
[12] Wang H, Zhou Y, Huang B, Liu LT, Liu MH, Wang J, Li CQ, Zhang ZF, Chu TW and Xiong CJ. Utilization of stem cells in alginate for nucleus pulposus tissue engineering. Tissue Eng Part A 2014; 20: 908-920.
[13] Zeng Y, Chen C, Liu W, Fu Q, Han Z, Li Y, Feng S, Li X, Qi C, Wu J, Wang D, Corbett C, Chan BP, Ruan D and Du Y. Injectable microcryogels reinforced alginate encapsulation of mesenchymal stromal cells for leak-proof delivery and alleviation of canine disc degeneration. Biomaterials 2015; 59: 53-65.
[14] Richardson SM, Walker RV, Parker S, Rhodes NP, Hunt JA, Freemont AJ and Hoyland JA. Intervertebral disc cell-mediated mesenchymal stem cell differentiation. Stem Cells 2006; 24: 707-716.
[15] Sakai D, Mochida J, Iwashina T, Watanabe T, Nakai T, Ando K and Hotta T. Differentiation of mesenchymal stem cells transplanted to a rabbit degenerative disc model: potential and limitations for stem cell therapy in disc regeneration. Spine (Phila Pa 1976) 2005; 30: 2379-2387.
[16] Watanabe A, Benneker LM, Boesch C, Watanabe T, Obata T and Anderson SE. Classification of intervertebral disk degeneration with axial T2 mapping. AJR Am J Roentgenol 2007; 189: 936-942.
[17] Gullbrand SE, Ashinsky BG, Martin JT, Pickup S, Smith LJ, Mauck RL and Smith HE. Correlations between quantitative T2 and T1rho MRI, mechanical properties and biochemical composition in a rabbit lumbar intervertebral disc degeneration model. J Orthop Res 2016; 34: 1382-1388.
[18] Chen C, Jia Z, Han Z, Gu T, Li W, Li H, Tang Y, Wu J, Wang D, He Q and Ruan D. Quantitative T2 relaxation time and magnetic transfer ratio predict endplate biochemical content of intervertebral disc degeneration in a canine model. BMC Musculoskelet Disord 2015; 16: 157.
[19] Mamisch TC, Hughes T, Mosher TJ, Mueller C, Trattnig S, Boesch C and Welsch GH. T2 star relaxation times for assessment of articular cartilage at 3 T: a feasibility study. Skeletal Radiol 2012; 41: 287-292.
[20] Stelzeneder D, Shetty AA, Kim SJ, Trattnig S, Domayer SE, Shetty V and Bilagi P. Repair tissue quality after arthroscopic autologous collagen-induced chondrogenesis (ACIC) assessed via T2* mapping. Skeletal Radiol 2013; 42: 1657-1664.
[21] Chen C, Huang M, Han Z, Shao L, Xie Y, Wu J, Zhang Y, Xin H, Ren A, Guo Y, Wang D, He Q and Ruan D. Quantitative T2 magnetic resonance imaging compared to morphological grading of the early cervical intervertebral disc degeneration: an evaluation approach in asymptomatic young adults. PLoS One 2014; 9: e87856.
[22] Perry J, Haughton V, Anderson PA, Wu Y, Fine J and Mistretta C. The value of T2 relaxation times to characterize lumbar intervertebral disks: preliminary results. AJNR Am J Neuroradiol 2006; 27: 337-342.
[23] Xie R, Ruan L, Chen L, Zhou K, Yuan J, Ji W, Jing G, Huang X, Shi Q and Chen C. T2 relaxation time for intervertebral disc degeneration in patients with upper back pain: initial results on the clinical use of 3.0 Tesla MRI. BMC Med Imaging 2017; 17: 9.
[24] Huang M, Guo Y, Ye Q, Chen L, Zhou K, Wang Q, Shao L, Shi Q and Chen C. Correlation between T2* (T2 star) relaxation time and cervical intervertebral disc degeneration: an observational study. Medicine (Baltimore) 2016; 95: e4502.
[25] Cai F, Wu XT, Xie XH, Wang F, Hong X, Zhuang SY, Zhu L, Rui YF and Shi R. Evaluation of intervertebral disc regeneration with implantation of bone marrow mesenchymal stem cells (BMSCs) using quantitative T2 mapping: a study in rabbits. Int Orthop 2015; 39: 149-159.
[26] Liu W, Li Y, Zeng Y, Zhang X, Wang J, Xie L, Li X and Du Y. Microcryogels as injectable 3-D cellular microniches for site-directed and augmented cell delivery. Acta Biomater 2014; 10: 1864-1875.
[27] Lee KH, No da Y, Kim SH, Ryoo JH, Wong SF and Lee SH. Diffusion-mediated in situ alginate encapsulation of cell spheroids using microscale concave well and nanoporous membrane. Lab Chip 2011; 11: 1168-1173.

[28] Ricks DM, Kutner R, Zhang XY, Welsh DA and Reiser J. Optimized lentiviral transduction of mouse bone marrow-derived mesenchymal stem cells. Stem Cells Dev 2008; 17: 441-450.
[29] Xin H, Zhang C, Wang D, Shi Z, Gu T, Wang C, Wu J, Zhang Y, He Q and Ruan D. Tissue-engineered allograft intervertebral disc transplantation for the treatment of degenerative disc disease: experimental study in a beagle model. Tissue Eng Part A 2013; 19: 143-151.
[30] Hiyama A, Mochida J, Iwashina T, Omi H, Watanabe T, Serigano K, Tamura F and Sakai D. Transplantation of mesenchymal stem cells in a canine disc degeneration model. J Orthop Res 2008; 26: 589-600.
[31] Lu DS, Shono Y, Oda I, Abumi K and Kaneda K. Effects of chondroitinase ABC and chymopapain on spinal motion segment biomechanics. An in vivo biomechanical, radiologic, and histologic canine study. Spine (Phila Pa 1976) 1997; 22: 1828-1834.
[32] Pfirrmann CW, Metzdorf A, Zanetti M, Hodler J and Boos N. Magnetic resonance classification of lumbar intervertebral disc degeneration. Spine 2001; 26: 1873.
[33] Yoon MA, Hong SJ, Kang CH, Ahn KS and Kim BH. T1rho and T2 mapping of lumbar intervertebral disc: correlation with degeneration and morphologic changes in different disc regions. Magn Reson Imaging 2016; 34: 932-939.
[34] Bechara BP, Leckie SK, Bowman BW, Davies CE, Woods BI, Kanal E, Sowa GA and Kang JD. Application of a semiautomated contour segmentation tool to identify the intervertebral nucleus pulposus in MR images. AJNR Am J Neuroradiol 2010; 31: 1640-1644.
[35] Nishimura K and Mochida J. Percutaneous reinsertion of the nucleus pulposus. An experimental study. Spine (Phila Pa 1976) 1998; 23: 1531-1538; discussion 1539.
[36] Chou AI, Akintoye SO and Nicoll SB. Photocrosslinked alginate hydrogels support enhanced matrix accumulation by nucleus pulposus cells in vivo. Osteoarthritis Cartilage 2009; 17: 1377-1384.
[37] Richardson SM, Hoyland JA, Mobasheri R, Csaki C, Shakibaei M and Mobasheri A. Mesenchymal stem cells in regenerative medicine: opportunities and challenges for articular cartilage and intervertebral disc tissue engineering. J Cell Physiol 2010; 222: 23-32.
[38] Menezes-Reis R, Salmon CE, Carvalho CS, Bonugli GP, Chung CB and Nogueira-Barbosa MH. T1rho and T2 mapping of the intervertebral disk: comparison of different methods of segmentation. AJNR Am J Neuroradiol 2015; 36: 606-611.
[39] Urban JP and Winlove CP. Pathophysiology of the intervertebral disc and the challenges for MRI. J Magn Reson Imaging 2007; 25: 419-432.
[40] Peeters M, Detiger SE, Karfeld-Sulzer LS, Smit TH, Yayon A, Weber FE and Helder MN. BMP-2 and BMP-2/7 heterodimers conjugated to a fibrin/hyaluronic acid hydrogel in a large animal model of mild intervertebral disc degeneration. Biores Open Access 2015; 4: 398-406.
[41] Chai JW, Kang HS, Lee JW, Kim SJ and Hong SH. Quantitative analysis of disc degeneration using axial T2 mapping in a percutaneous annular puncture model in rabbits. Korean J Radiol 2016; 17: 103-110.
[42] Vadala G, Russo F, Ambrosio L, Loppini M and Denaro V. Stem cells sources for intervertebral disc regeneration. World J Stem Cells 2016; 8: 185-201.
[43] Raj PP. Intervertebral disc: anatomy-physiology-pathophysiology-treatment. Pain Pract 2008; 8: 18-44.
[44] Marinelli NL, Haughton VM, Munoz A and Anderson PA. T2 relaxation times of intervertebral disc tissue correlated with water content and proteoglycan content. Spine (Phila Pa 1976) 2009; 34: 520-524.
[45] Sun W, Zhang K, Zhao CQ, Ding W, Yuan JJ, Sun Q, Sun XJ, Xie YZ, Li H and Zhao J. Quantitative T2 mapping to characterize the process of intervertebral disc degeneration in a rabbit model. BMC Musculoskelet Disord 2013; 14: 357.
[46] Minogue BM, Richardson SM, Zeef LA, Freemont AJ and Hoyland JA. Characterization of the human nucleus pulposus cell phenotype and evaluation of novel marker gene expression to define adult stem cell differentiation. Arthritis Rheum 2010; 62: 3695-3705.
[47] Takashima H, Takebayashi T, Yoshimoto M, Terashima Y, Tsuda H, Ida K and Yamashita T. Correlation between T2 relaxation time and intervertebral disk degeneration. Skeletal Radiol 2012; 41: 163-167.
[48] Priyadarshani P, Li Y and Yao L. Advances in biological therapy for nucleus pulposus regeneration. Osteoarthritis Cartilage 2016; 24: 206-212.
[49] Han Z, Gao L, Shi Q, Chen L and Chen C. Quantitative magnetic resonance imaging for diagnosis of intervertebral disc degeneration of the cervico-thoracic junction: a pilot study. Am J Transl Res 2018; 10: 925-935.
[50] Chen P, Wu C, Huang M, Jin G, Shi Q, Han Z and Chen C. Apparent diffusion coefficient of diffusion-weighted imaging in evaluation of cervical intervertebral disc degeneration: an observational study with 3.0 T magnetic resonance imaging. Biomed Res Int 2018; 2018: 6843053.

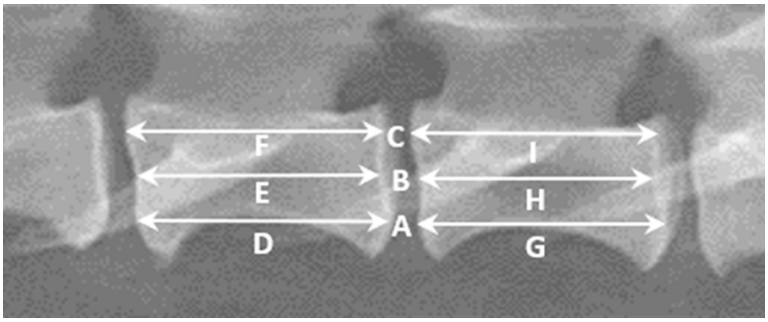

Figure S1. Schematic measurement of the change of disc height. DHI, disc height index.

Table S1. MRI parameters

Sequence	T1W FSE sagittal	T2W FSE sagittal	T2 map sagittal
Repetition time (ms)	580	2500	1500
Echo time (ms)	Min Ful	108.9	8.5-67.9
Field of view (mm)	24 × 24	24 × 24	20 × 20
Slices	7	10	64
Interslice gap (mm)	0.3	0.3	0.6
Slice thickness (mm)	3	3	3
Image matrix	320 × 224	320 × 224	256 × 160
Echo trains/slice	2	18	-
Examination time (s)	125	186	267

MRI, magnetic resonance imaging; T1W FSE, T1-weighted fast spin echo sequence; T2W FSE, T2-weighted fast spin echo sequence.

Table S2. Histological grading system of disc degeneration based on the inner annulus fibrosus structure

Grade	The structure of the inner annulus fibrosus
Grade 0	Normal
Grade 1	Mildly serpentine appearance with rupture
Grade 2	Moderately serpentine appearance with rupture
Grade 3	Severely serpentine appearance with mildly reversed contour
Grade 4	Severely reversed contour
Grade 5	Indistinct

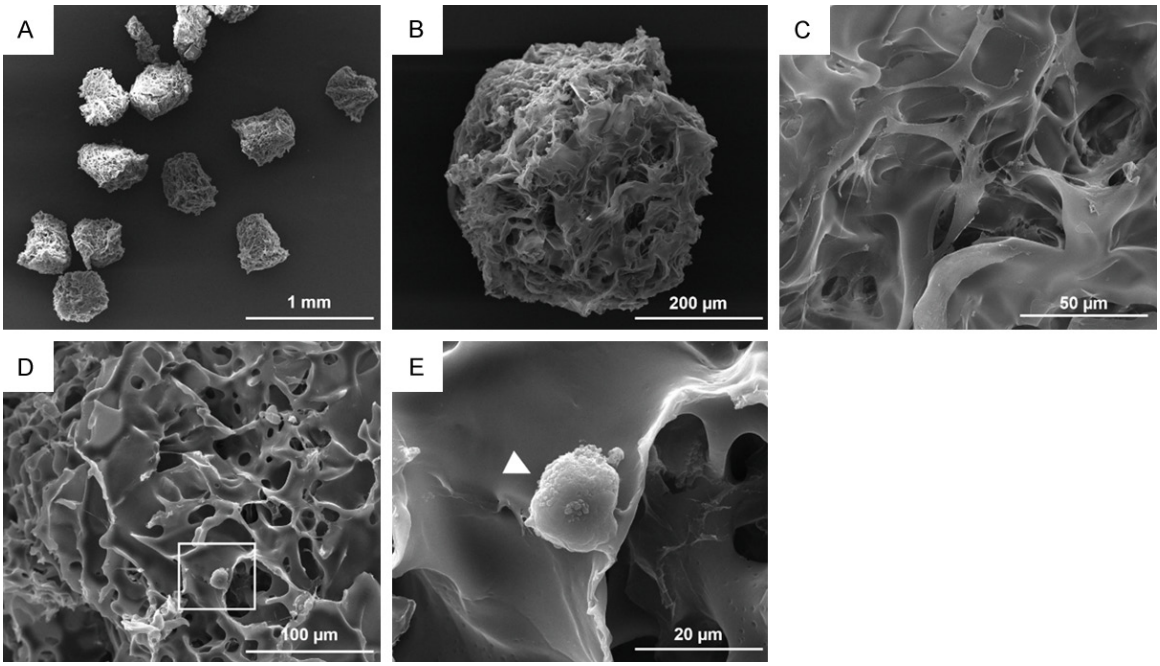

Figure S2. Structural characteristics of PMs. A-C. SEM images illustrating interconnected macroporous structures of PMs at different magnifications. PMs has the potential to improve the mechanical property by providing AH with skeletal network. D, E. A rounded cell (arrow head) tightly attaching the inner wall of PMs after loading cell-AH mixture. The 3D microscale cellular niches could provide cell with an appropriate microenvironment. PMs, PEGDA-microcryogels; SEM, scanning electron microscope; AH, alginate hydrogel.

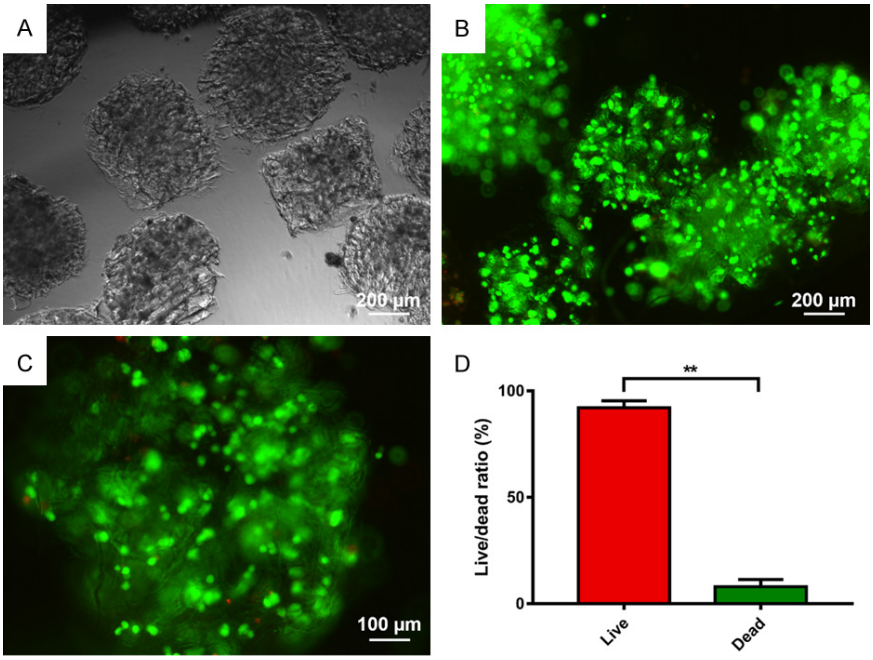

Figure S3. Live/dead staining assessing cell viability after 7-day culture *in vitro*. A. Microscopic image of MSCs-loaded AH-PMs in PBS before injection. B, C. Green indicates live cells while red indicates dead cells. The loaded cells were uniformly distributed in PMs reinforced AH. D. The comparison of percentages of live and dead cells in AH-PMs. The mean percentage of live cells was 92.3% and the mean percentage of dead cells was 7.7%. MSCs, mesenchymal stem cells; AH, alginate hydrogel; PMs, PEGDA-microcryogels; PBS, phosphate-buffered saline. All data are expressed as mean ± SD, n = 3. ** indicates $P < 0.001$.

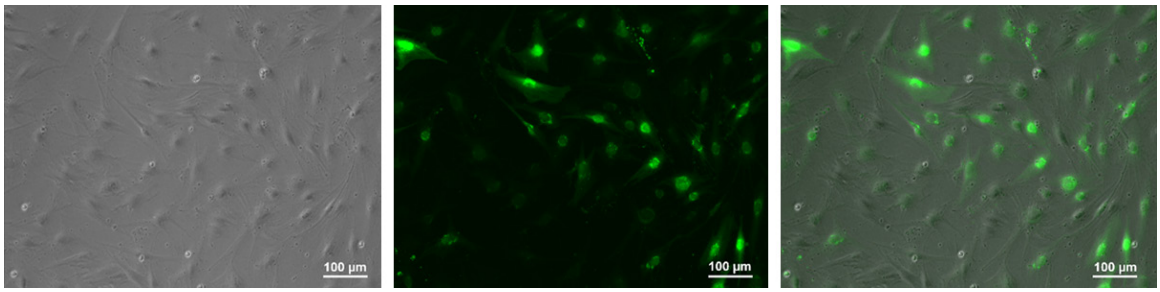

Figure S4. Representative photographs demonstrating successful transfection with lentiviruses to express GFP in adipose-derived MSCs. MSCs, mesenchymal stem cells; GFP, green fluorescent protein.

Table S3. Comparisons of the expression levels of PG and COL II among the different groups using ELISA analysis

(pg/mg)	NC	Sham	MSCs	AH-PMs	MSCs + AH-PMs
PG	214.9 ± 43.5**	72.2 ± 11.4	105.0 ± 13.1$^{\&}$	101.8 ± 13.9$^{\#}$	129.3 ± 27.5$^{@@}$
COL II	176.6 ± 17.0**	61.0 ± 10.6	89.2 ± 10.5$^{\&\&,\Delta}$	82.0 ± 12.2$^{\#,\nabla\nabla}$	113.9 ± 23.4$^{@@}$

NC, normal control; MSCs, mesenchymal stem cells; AH, alginate hydrogel; PMs, PEGDA-microcryogels; PG, proteoglycan; COL II, collagen II; ELISA, enzyme-linked immunosorbent assay. "*" indicates normal group compared to other groups, $^{**}P < 0.001$; "&" indicates MSCs group compared to sham group, $^{\&}P < 0.05$, $^{\&\&}P < 0.001$; "#" indicates AH-PMs group compared to sham group, $^{\#}P < 0.05$; "@" indicates MSCs + AH-PMs group compared to sham group, $^{@@}P < 0.001$; "Δ" indicates MSCs group compared to MSCs + AH-PMs group, $^{\Delta}P < 0.05$; "∇" indicates AH-PMs group compared to MSCs + AH-PMs group, $^{\nabla\nabla}P < 0.001$.